Large-scale extrusion processing and characterization of hybrid nylon-6/SiO2 nanocomposites

Garcia, M; van Vliet, G; ten Cate, MGJ; Chavez, F; Norder, B; Kooi, B; van Zyl, WE; Verweij, H; Blank, DHA; Cate, Mattijs G.J. ten

Published in:
Polymers for Advanced Technologies

DOI:
10.1002/pat.458

Publication date:
2004

POLYMERS FOR ADVANCED TECHNOLOGIES
Polym. Adv. Technol. 2004; **15**: 164–172
Published online in Wiley InterScience (www.interscience.wiley.com). DOI: 10.1002/pat.458

PAT

Large-scale extrusion processing and characterization of hybrid nylon-6/SiO_2 nanocomposites

Monserrat García[1]*, Gerhard van Vliet[2], Mattijs G. J. ten Cate[1], Francisco Chávez[3], Ben Norder[4], Bart Kooi[5], Werner E. van Zyl[1†], Henk Verweij[1] and Dave H. A. Blank[1]

[1]Faculty of Science and Technology and MESA$^+$ Research Institute, University of Twente, P.O. Box 217, 7500 AE Enschede, The Netherlands
[2]DSM Research, Material Science Center, P.O. Box 18, 6160 MD Geleen, The Netherlands
[3]Department of Chemical Engineering, Princeton University, Princeton, NJ 08544, USA
[4]Polymer Materials and Engineering, Faculty of Applied Sciences, Delft University of Technology, Julianalaan 136, 2628 BL Delft, The Netherlands
[5]Department of Applied Physics, University of Groningen, 9747 AG Groningen, The Netherlands

Received 30 July 2003; Revised 23 October 2003; Accepted 24 November 2003

Solution impregnations, pulltrusion and film stacking are widely used methods to prepare thermoplastic composite materials. Extruders are used to melt the polymer and to incorporate fibers into the polymer in order to modify physical properties. In this article, the compounding of colloidal silica nanoparticles filled polyamide-6 (PA-6) is achieved using a twin-screw extruder, which has a significant market share due to its low cost and easy maintenance. The experiments were performed at 250 rpm and the bulk throughput was 6 kg h^{-1} with a pump pressure of 30 bars. The composites were characterized with nuclear magnetic resonance (NMR), wide angle X-ray diffraction (WAXD), differential scanning calorimetry (DSC) and transmission electron microscopy (TEM). As determined by WAXD, the PA-6 showed higher amounts of γ-phase when compared to other synthesis methods such as *in situ* polymerization. TEM pictures showed that the silica particles aggregated nevertheless, upon addition of 14% (w/w) silica the E-modulus increased from 2.7 to 3.9 GPa indicating that an effective mechanical coupling with the polymer was achieved. The behavior, illustrated with dynamic mechanical analysis (DMA) curves, indicated that in general when a filled system is compared to unfilled material, the values of the moduli (E′ and E″) increased and tan δ decreased. Determination of molecular mass distribution of the samples by means of size exclusion chromatography (SEC) coupled to a refractive index (RI), viscosity (DV) and light scattering (LS) detector revealed that the addition of silica did not decrease the average molecular weight of the polymer matrix, which is of importance for composite applications.

KEYWORDS: nanocomposites; nylon-6/silica system; NMR; differential scanning calorimetry (DSC); screw-extrusion

INTRODUCTION

The ability to engineer nanometer-sized materials has potential for important applications as shown by Toyota Motor Co., who demonstrated the first practical example of polymeric nanocomposites used in the automotive industry.[1] The incorporation of nano-fillers into polymeric matrices produce higher levels of stiffness and/or toughness in structural engineering materials. These nanostructured materials often exhibit combinations of physical and mechanical properties that are not achievable with conventional materials. Because of their high adsorption energies and high surface-to-volume ratio, nanoparticles in composites offer a range of new materials with useful combinations of properties.[2]

*Correspondence to: M. García, Faculty of Science and Technology and MESA$^+$ Research Institute, University of Twente, P.O. Box 217, 7500 AE Enschede, The Netherlands.
E-mail: m.m.garciacuriel@utwente.nl
†Department of Chemistry and Biochemistry, Rand Afrikaans University, P.O. Box 524, Auckland Park 2006, South Africa.

During the past few decades polyamide-6 (PA-6) has occupied a prominent position in engineering thermoplastics due to its wide spectrum of properties.[3] The mechanical properties of PA-6 can be modified by the addition of inorganic fillers.[4] Fillers widely used are calcium carbonate, talc, silica and glass fibre, which play an important role in the plastics filler market.[5] The influence of these fillers on the polyamide strongly depends on their shape, particle size, distribution and surface characteristics. A composite with improved properties and a low particle concentration (to preserve properties of pure matrix) is desired. Since silica (SiO_2) is very versatile,[6] it is one of the most applied fillers in thermoplastic polymer composites and it has also been applied in electrical engineering, electronics, appliances and consumer goods.[7] Presently, polymer composites of PA-6 and nanosilica have been prepared by *in situ* polymerization where inorganic particles are dispersed in ε-caproamide and aminocapric acid, followed by heat treatment of the reaction mixture to induce polymerization, and post-addition of solid

silica[4,8] (modified or unmodified) and *in situ* polymerization of the inorganic fillers, where silica sol is added to caprolactam and mixed into a reactor.[9] The most prominent physical effect of fillers is the stiffening or modulus increase in the composites. Colloidal silica has been also added to reinforce polyurethane prepared by mixing polyol with the filler and subsequent curing using di-isocyanate. The investigation showed that at low temperatures (below $-40^{\circ}C$) the addition of nanoparticles at 10 vol% increased the storage modulus of the polymer, but at room temperature an opposite effect was observed.[10] Both the moduli and Poisson's ratio, ν, of the material are influenced since the fillers are generally much more rigid than polymers. Due to the manner in which test specimens are usually molded, at a certain filler percentage aggregation will occur. However, agglomerates or flocculated particles can provide higher modulus,[11] since that portion of the matrix which is isolated in the agglomerate is less free to react to stress and strain than the continuous phase at values below the maximum packing fraction P_f. Under conditions where the particles have been treated with coupling agents, the matrix is severely restricted by interfacial bonding, so tensile strengths are improved and elongations are reduced. Agglomerated particles have been assumed to behave as a rigid unit under the action of small stress, but above some critical stress, relative motion of the particles within the agglomerate can occur.[11] Sumita *et al.*[12] have reported the advantages of nano- over micro-sized particles almost two decades ago, and investigations for the optimal preparation and processing for the enhancement of mechanical properties are ongoing. For example, in the suspension process where (microsized) solid particles pass through a suspension state brought in contact with the granules of the thermoplastic, proved to be an effective way to make composites for large-scale extrusion.[13]

In this article the preparation of PA-6 silica nanocomposites is reported. The nano-composites present a primary particle size of 30 nm, and were made by the devolatilization method in a twin-screw extruder. The process is particularly trouble-free where colloidal nanosized silica particles and polyamide pellets are used, and it furthermore leads to better modulus values compared to those obtained by common methods. The effect of the nanofiller on the modulus of PA-6 is discussed and compared with the theoretical models available in the literature.

EXPERIMENTAL

Materials

PA-6 Akulon K122 (relative viscosity = 2.2) was provided by DSM (Geleen, The Netherlands). Colloidal silica ST-0, with a particle size of 10–20 nm and viscosity <3 mPa sec. at 25°C was provided by SNOWTEX® Chemical Europe GmbH (Düsseldorf, Germany). Silica additions of 0, 1.85, 3.2, 7 and 14 wt% were used. The samples were labelled as PA0, PA1, PA3, PA7 and PA14, respectively.

Processability

The compounding of the PA-6/nanoSiO_2 composites was performed feeding the colloidal (silica) in a high-pressure reaction zone. The process was developed on a ZSK-30 twin-screw extruder. An important parameter was the addition mixing of the silica to the molten polymer: the water, in which the silica was dissolved, should not evaporate. Therefore, conditions to be fulfilled were (a) the pressure in the mixing zone should be higher than the vapor pressure of the water, and (b) the pressure drop (passage of the melt through the left handed elements) should be faster than the destabilizing foam forming process (devolatilization). The pressure drop prevented pressure fluctuations and instabilities to occur in the throughput. The screw of the extruder was designed with a reaction zone for mixing the PA-6/silica with different filler loadings. The use of a dynamic seal increased the pressure in the reaction zone and resulted in a stable process (Fig. 1a). A detailed photograph of the dynamic seal is showed in Fig. 1(b). A real-melt thermocouple (the sensor was placed in the melt between the two screws, which were interrupted by spacers) and a pressure transducer monitored the temperature and the pressure in the 'reaction-zone'. The experiments were performed at 250 rpm and the throughput was 6 kg hr^{-1} with a pump pressure of 30 bar.

Characterization methods

Solution ^1H- and ^{13}C-NMR spectra were recorded on a Varian Unity 400 (300 MHz) spectrometer. Equilibrium thermodynamic parameters were determined using a Perkin–Elmer differential scanning calorimeter (DSC-7), under a nitrogen atmosphere. Sample weights were between 5–10 mg. The samples were heated (at 10°C min^{-1}) to 20–30°C above the melting temperature, remained there for 10 min to eliminate residual crystals, then cooled to room temperature at a rate of 10°C min^{-1}. All the scans were recorded between 23 and 250°C, and a heating rate of 10°C min^{-1} was used for all the scans. The differential scanning calorimetry (DSC) measurements were performed according to DIN 51007/53765 and ASTM D3417-97 protocol. The dynamic mechanical spectra were recorded on a Perkin–Elmer DMA 7E Dynamic Mechanical Analyzer. Small rectangular bars of the samples, size approximate $1.25 \times 3 \times 20\,mm^3$, were subjected to a sinusoidal deformation at constant frequency, using a three point bending platform of 15 mm. Measurements were carried out at a fixed frequency of 1 Hz and a heating rate of 5°C min^{-1}, in the temperature range between −100 and 200°C. The amplitude of the sinusoidal deformation was 10 μm during the run. The static force was always 10% more than the dynamic force, in order to ensure good contact between the probe and the sample. The data was collected using Pyris software for Windows, version 3.81.

Prior to the dynamic mechanical analysis (DMA) measurements, the samples were compression molded into sheets of size $30 \times 5.5 \times 0.1\,cm^3$ at 250–260°C. Prior to testing, sample strips of $25 \times 2–3 \times 0.05–0.1\,cm^3$ were made. For the tensile test, the samples were dried in a vacuum oven at 80°C for 2 days. Plates of 1 mm thickness were molded and the test samples were machined out of the plates. The elastic modulus was measured at a tensile speed of 1 mm min^{-1} and the displacement was measured with an extensometer with a gauge length of 10 mm. Yield stress,

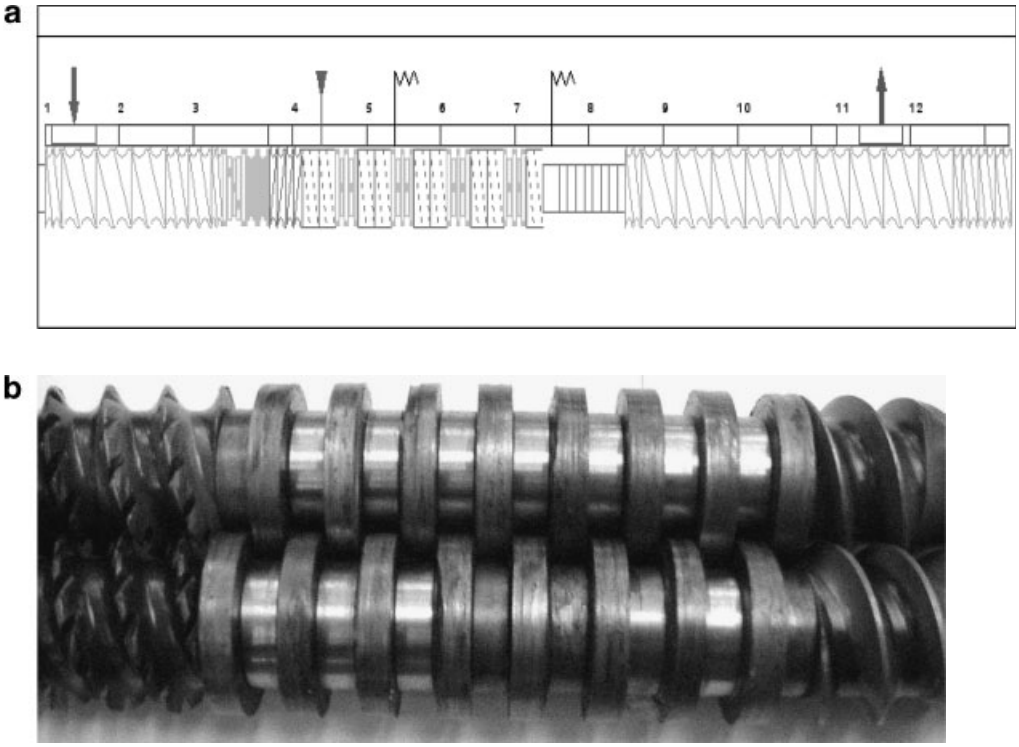

Figure 1. Screw configuration with high pressure mixing zone for water injection and venting zone. Dynamic seal consist of standard left-handed elements (a) or blister-discs (b).

strain-at-yield and strain-at-break were recorded on a Zwick Z010 apparatus.

X-ray powder diffraction (XRD) data were collected using copper radiation on a Philips PW3710 based X'Pert-1 diffractometer in Bragg–Brentano geometry. The K_β component was removed by a secondary monochromator. Powder diffraction data were collected at room temperature using a 'zero'-background spinning specimen holder. The intensities were measured using a θ compensating divergence slit. The measured data were converted to a fixed divergence slit width of 1°. Peak positions and peak intensities were extracted using the pattern decomposition program PROFIT available in the PC software package X'PERT LINE (Philips, Eindhoven). The observed individual lines and clusters of lines were fitted using Pearson VII functions, taking into account the $K\alpha_2$ component. The obtained peak positions and relative intensities were therefore extracted from the analytical $K\alpha_1$ peak profiles. Quantitative X-ray fluorescence (XRF) was used to determine the amount (as wt%) of silica present in each sample. The XRF analysis was performed on a Philips PW 1480/10 fluorometer (Eindhoven, The Netherlands) and the calculation method used the program FPMulti.

For transmission electron microscopy (TEM) studies, a JEOL 2010F operating at 200 kV, equipped with a EDAX-EDS detector and a Gatan Imaging Filter, was used. TEM specimens were prepared by embedding the PA-6/silica composite in Epon, cutting it into thin films with a thickness of 100 nm using ultramicrotomy after which the films could be captured on Cu grids. TEM images were recorded on a Gatan DualVision 300 W CCD camera.

Mechanical properties of injection molded PA-6 nanocomposites

The specimens for the tensile tests were dog-bone shaped samples which were injection molded in a $\phi = 30$ mm Engel 80A machine set up according to the ISO 527 standard and functioned at 100 rpm. The melt temperature was 270°C and the mold-temperature 85°C. The raw materials were dried overnight at 110°C in vacuum prior to injection molding. The prismatic part of the tensile samples had dimensions $60 \times 10 \times 4.2\,mm^3$. The tensile modulus was determined between 0.05 and 0.25% strain according to DIN-53457 protocol at 23°C and 5 mm min^{-1}.

RESULTS AND DISCUSSION

NMR analysis and molecular parameters

Figure 2 shows the ^{1}H-NMR spectra of the formed composites. Concentrations of 70 mg polymer per ml were used to perform the experiment. ^{1}H-NMR spectra of neat polymer and composite showed a chemical shift of hydrogen-bonded protons at 12.3 ppm. Chemical shifts of the CH_2 groups adjacent to the NH group and CO group were observed around 3.6 and 2.8 ppm, respectively. Chemical shifts of the remaining aliphatic CH_2 protons were observed around 1.9 ppm (4H) and 1.6 ppm (2H). ^{13}C-NMR spectrometry of neat polymer and composite gave a peak at 179 ppm corresponding to the carbon of the amido group (Fig. 3). The peaks at 42 and 33 ppm correspond to the carbon atoms next to the amido groups (i.e. $-CONHC^*H_2-$ and $-C^*H_2CONH-$, respectively), whereas the signals at 26, 25 and 24.5 ppm

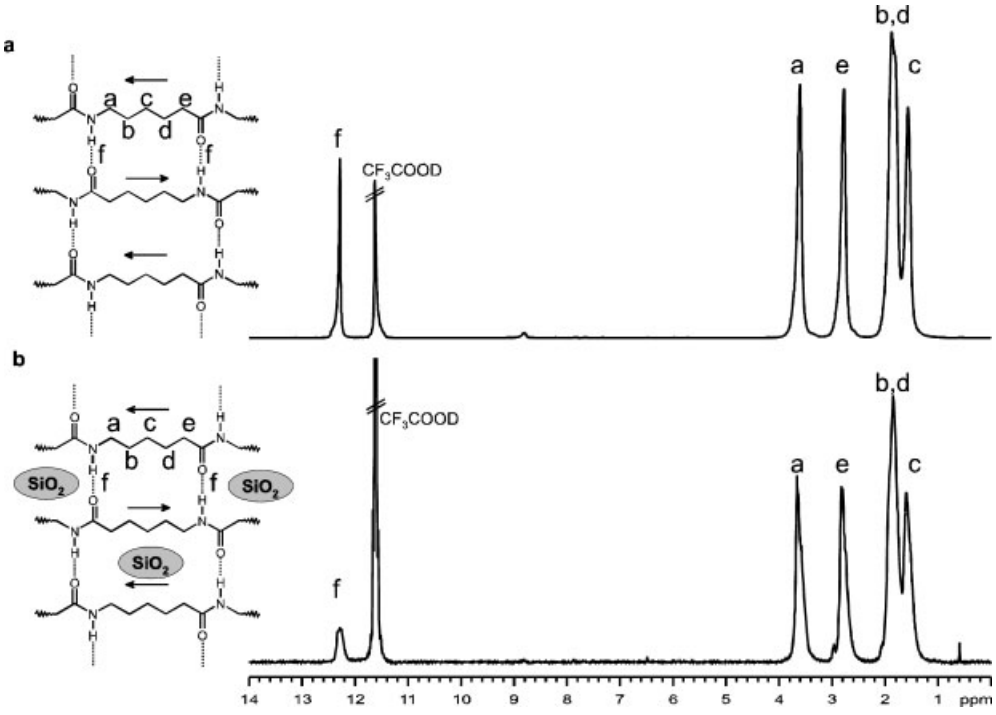

Figure 2. Solution ^{1}H-NMR spectra of (a) PA-6, (b) PA-6/SiO_2 in CF_3COOD.

belong to the remaining aliphatic carbon atoms. ^{1}H- and ^{13}C-NMR spectra of the composites were in complete accordance with the anticipated chemical structure for PA-6.[14]

Besides the morphology of the matrix and characteristics of the filler, the properties of the plastics depend also on the matrix molecular weight (M_w) of the polymer. The effects of PA-6 molecular weight stems from both chemical and rheological issues. The molecular weight can potentially affect the toughness in different ways. In general, the inherent ductility, or the ability for the polymer to be toughened, increases with molecular weight and therefore a matrix with a molecular weight above 30 000 g/mol was chosen. At high silica loadings (14 wt%) the viscosity slightly varied from 1.36 to 1.37 dl/g and the molecular weight was not decreased as seen in Table 1.

XRD and DSC experiments

To calculate the crystallinity from a XRD scan the method based on the use of amorphous templates was used.[3] The

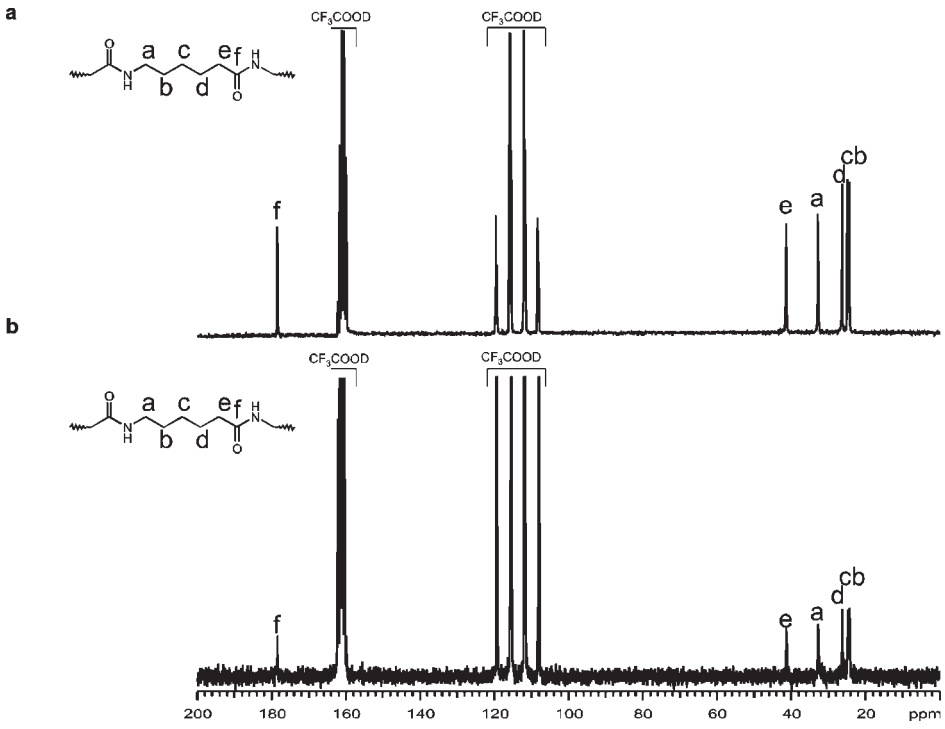

Figure 3. Solution ^{13}C-NMR spectra of (a) PA-6, (b) PA-6/SiO_2 in CF_3COOD.

Table 1. Molecular structure parameters of PA0 and PA14 as obtained from SEC-triple molecular weight (in g/mol) and [η] (in dl/g)

Sample name	M_n	M_w	M_z	M_w/M_n	M_z/M_w	Intrinsic viscosity	Mark–Houwink slope 'a'
PA0	17 100	35 400	56 500	2.07	1.60	1.362	0.641
PA14	19 600	42 600	71 200	2.17	1.67	1.378	0.643

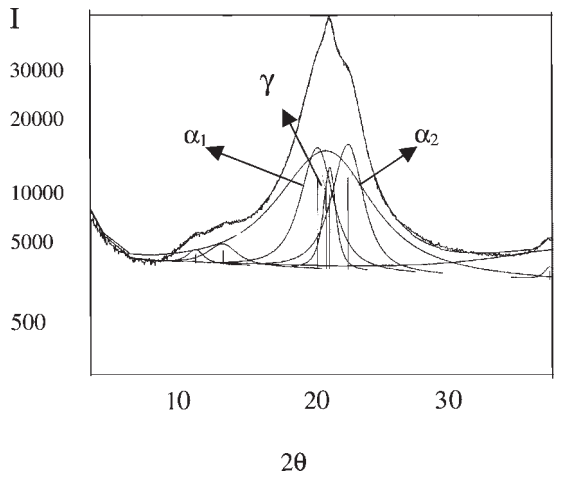

Figure 4. Profile analysis of the diffraction scan from PA0 indicating relevant phases.

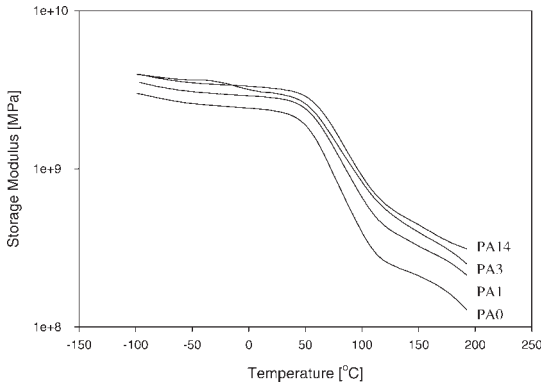

Figure 6. *E′* relaxations of PA0, PA1, PA3 and PA14.

amorphous template was derived by stripping the crystalline peaks from a resolved pattern of a highly crystalline sample of the same polymer. From Fig. 4 three components are observed consisting of α_1, α_2 and γ-form crystal diffraction peaks centred at $2\theta = 20.3^\circ$, 22.6° and 21.2°, respectively. The amorphous component was taken from the areas below the α-form crystal peaks and the γ-form crystal peak. The crystallization and melting behavior of the composites has been studied by DSC analysis.

From the DSC heating curves in Fig. 5, the influence of silica on the melting temperature (T_m) and on the crystallization temperature was observed. Pure PA0 showed a $T_m = 225.3^\circ$C as seen in Fig. 5(a). This melting temperature is typical for α-polyamides. At higher silica loadings, the melting temperature was shifted towards lower temperatures while at the same time a second peak at around 213°C emerged at temperatures below the normal melting temperature of PA-6

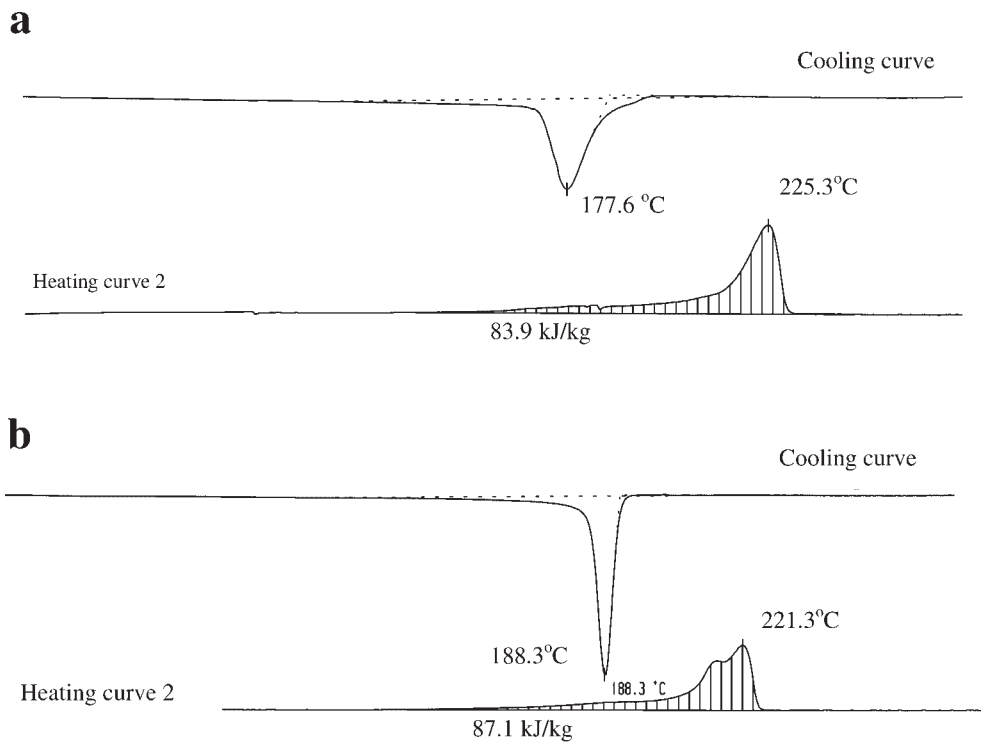

Figure 5. Crystallization enthalpies and melting temperatures of the nanocomposites. (a) PA0; (b) PA14.

Table 2. Differential scanning calorimetry (DSC) data of the samples

Sample name	SiO_2 (wt%)	T_{m1} (°C)	ΔH_{m1} (kJ kg^{-1})	T_{m2} (°C)	ΔH_{m2} (kJ kg^{-1})	T_c (°C)
PA0	0	227.2	76.1	225.3	83.9	177.6
PA1	1.85	223.6	79.5	220.4	73.3	189.1
PA3	3.2	223.3	79.5	220.7	69.8	188.3
PA7	7	223.0	74.5	220.7	66.3	188.9
PA14	14	223.0	78	221.3	67.1	188.3

(Fig. 5b). Such temperature is typical for γ-crystalline PA-6, which is in agreement with the results obtained from the XRD spectra. Melting and crystallization peak-temperatures (T_c and enthalpies are listed in Table 2. The melting temperature decreased upon addition of particles and this can probably be attributed to a decrease in lamellar thickness of the polymer crystals. The degree of crystallinity was determined from the enthalpy of melting as:

$$W_c = \frac{\Delta h_f}{\Delta h_f^0} \quad (1)$$

where Δh_f is the experimentally measured enthalpy of melting and Δh_f^0 the bulk enthalpy of melting, respectively. The heat of fusion for PA-6 was taken as 188 J g^{-1} for the crystalline fraction.[3] Upon addition of silica nanoparticles, the degree of crystalliny did not vary significantly which was in accordance with the XRD experiments. The silica had two effects on the crystallization of PA-6:[15] (1) the silica acts as a nucleation site, accelerating the process of PA 6 crystallization; (2) the interaction between PA-6 and the silica impedes the free motion of the PA 6 molecular chains (this effect is more pronounced when the silica surface is modified).[15] The experimental results from NMR to some extent support the view that the silica impeded the mobility of chain units. By using techniques such as the NMR relaxation time or quasi-elastic neutron scattering (QENS) it is possible to characterize the dynamic restrictions of polymer chains in polymer-filler composites.[16]

Dynamic mechanical analysis (DMA)

Modulus and tan δ for the silica particles in the polyamide matrix are measured as a function of temperature for several values of volume fraction of filler. Figure 6 shows data for the storage modulus (E'), Fig. 7 for the loss modulus (E'') and Fig. 8 the tan δ or damping values. For the storage modulus below the glass transition temperature (T_g), log E' decreased linearly with temperature and about 20°C below the T_g decreased with nearly one order of magnitude. As expected, the storage modulus curve shifted to higher modulus upon addition of 1 and 3 wt% of silica. Upon addition of 14 wt% the increment was not significant anymore. The addition of 5 and 7 wt% of silica caused an increase in modulus between the values of 3 and 14 wt%. For clarity only PA1, PA3 and PA14 composites are shown. However, because of the presence of a crystalline matrix, the material does not drastically soften above the glass transition. Above the T_g the mobility of the amorphous regions caused a reduction in the storage modulus, but the material exhibited useful solid-state properties until the material approached the melting point, about 100°C above the glass transition. As seen from Fig. 7, the T_g does not change significantly with increasing filler content. The rise in the tan δ curve coincided with the decline in the storage modulus as seen in Fig. 8. Above 60°C the tan δ curve rose rapidly and reached a peak of 0.6. Once the T_g value is passed; the loss modulus drops back to a level close to the pre-transition values. However, because of the drastic reduction in elastic properties, the tan δ curves do not decline significantly. Once the semi-crystalline material approached the melting point, the tan δ value increased as the material changed from an elastic solid into a viscous liquid. The lower tan δ values throughout the scan, and in particular the lower peak associated with the glass transition, reflected the improved load bearing properties of the filled system. One transition is observed at about −40°C, which corresponds to the secondary relaxation. In addition, at about 50–60°C the α-relaxation is visible, corresponding to the T_g value of the matrix.

The damping can be explained as follows: below the T_g value part of the decrease in relative damping as the temperature was raised may be due to the frozen-in stresses caused by the mismatch in the coefficients of thermal expansion of the two materials or to a decrease in motion of particles within agglomerates as the polymer softens.[17] The

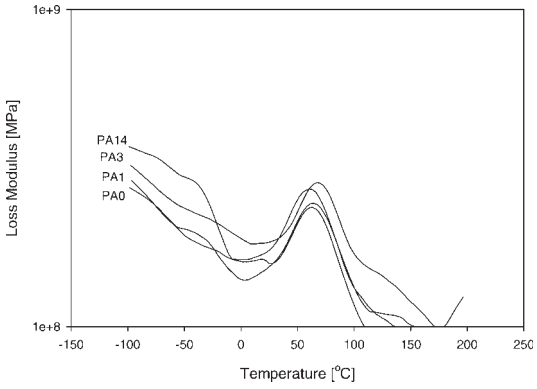

Figure 7. E'' relaxations of PA0, PA1, PA3 and PA14.

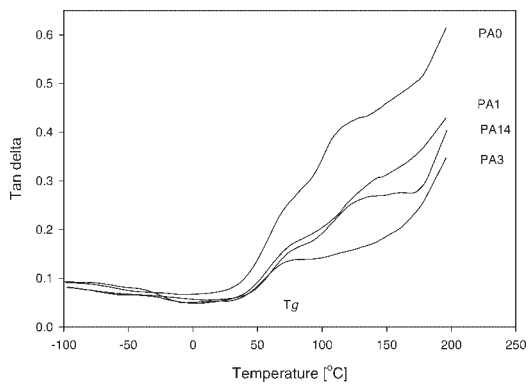

Figure 8. Tan δ relaxations at different filler percentage.

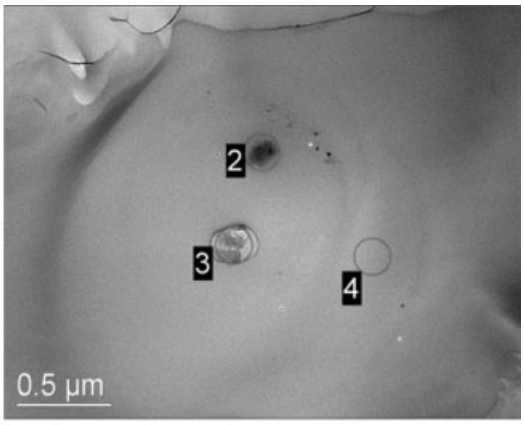

a

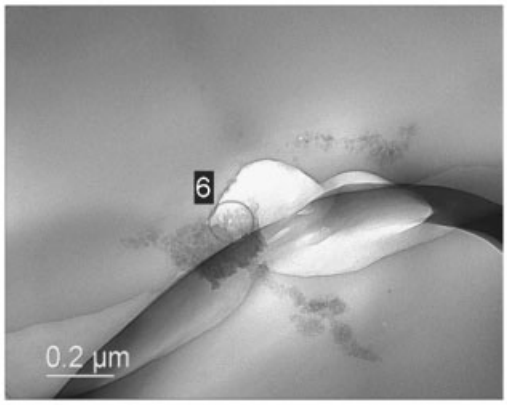

b

Figure 9. (a) TEM picture of PA3; (b) Magnification of (a).

microstructure of the nanocomposite is seen in Figs. 9(a) and 9(b). The silica nanoparticles showed a primary particle size of 30 nm as observed by TEM. The presence of silica was confirmed by using EDAX-EDS as shown in Fig. 10. (The number 2, 3 and 6 indicate aggregated silica.) As the modulus

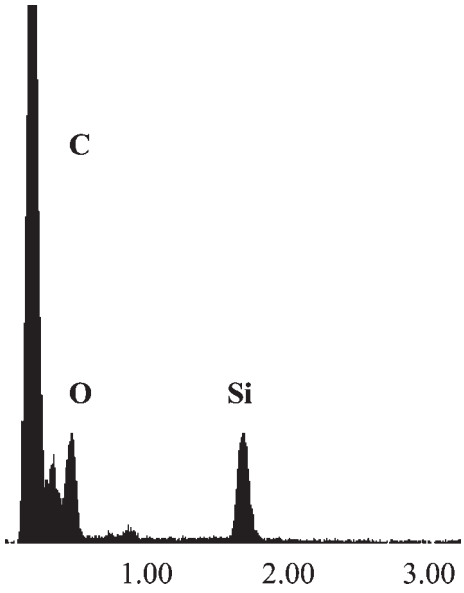

Figure 10. Energy dispersive spectrum (EDAX-EDS) of PA3.

of the polymer decreased on raising the temperature, the polymer exerted less force on the agglomerate particles, so there was a smaller probability that one primary particle will move with respect to another within agglomerates.[18] In the neighborhood of T_g, the modulus of the polymer decreased to such a small value that deformation of the material no longer produces forces large enough to deform agglomerate particles, so they appear to be rigid. At this point, the relative damping is small since most of the damping originates from the polymer.

Beyond the T_g, damping increased at higher temperatures because the coefficient of thermal expansion of the polymer is much greater than of the filler and the polymer exerts less force on the agglomerate particles as temperature increases. As the force between the polymer and the filler particles decreased, it became more facile for either polymer-filler or filler-filler motion to occur at the interfaces. This frictional motion at interfaces generates heat that produces an increase in the relative damping as the temperature increases.

As mentioned earlier, the change in relative modulus with temperature is primarily due to induced tensile stresses by the difference in thermal expansion coefficient of the phases.[18] For a single sphere in a matrix, the stress at a distance r from the centre of the particle of radius R is:[19]

$$\sigma = \sigma* (R/r)^3 \tag{2}$$

where $\sigma*$ is the thermally induced tensile stress at the interface. In general, an average stress $\bar{\sigma}$ in the matrix can be determined as:

$$\bar{\sigma} = \int \sigma \mathrm{d}V / \int \mathrm{d}V = f(\phi_2)\sigma* \tag{3}$$

where $f(\phi_2)$ is a function of ϕ_2, the volume fraction of the filler, and depends on the nature of the stress fields around the particles, and V is a volume element.

Mechanical models

The effects of the silica content on the mechanical properties of the nylon-6/silica composites are seen in Figs. 11 and 12. From the minimum potential energy in elasticity theory it is possible to obtain bounds for the elastic properties of a composite material.[20] Nielsen provided a generalization of these bounds:[21]

$$C^n = \phi_\mathrm{f} C_\mathrm{f}^n + (1 - \phi_\mathrm{f}) C_\mathrm{m}^n \tag{4}$$

where C stands for either the bulk modulus k, or the shear modulus, μ, the sub-index f represents the filler properties, the sub-index m the matrix properties, and ϕ_f represents the volume fraction of the filler. Quantities without any sub-index refer to the properties of the composite. Different values of the exponent n give rise to different forms of the law of mixtures. With $n = -1$, eqn. (4) is referred to as the series law of mixtures or the Reuss lower bound. With $n = 1$, eqn. 4 is referred to as the parallel law of mixtures or the Voigt upper bound. A comparison of these bounds with the measured moduli for the composites considered in this work are shown in Fig. 11. Although these bounds provide theoretical limits for the values of the moduli, for typical composite materials they are too far apart and are thus of limited practical value.

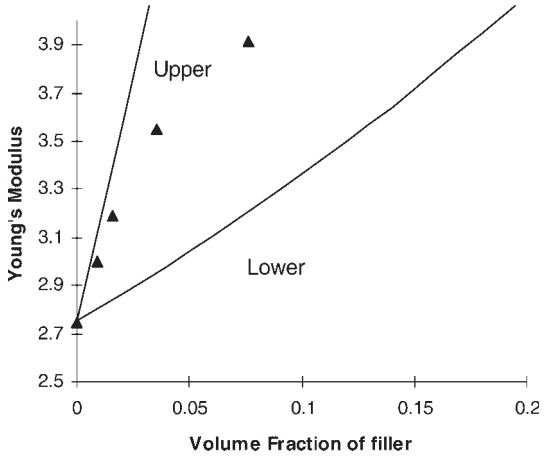

Figure 11. Experimental Young's modulus (symbols) and theoretical upper and lower bounds (solid lines) for the Akulon K122 polymer reinforced with nanosilica particles.

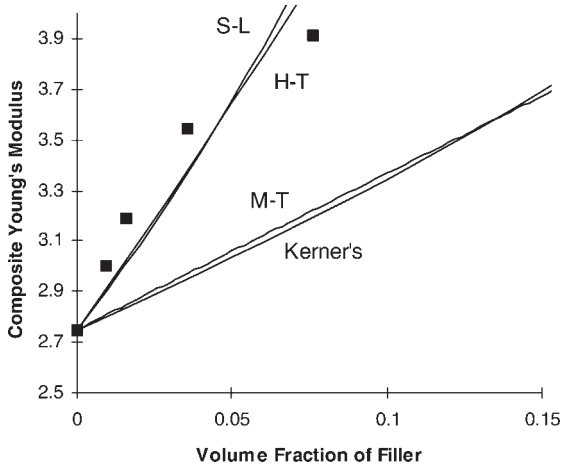

Figure 12. Experimental Young's modulus from experimental measurements (symbols) and micromechanical models (solid lines): M–T, Mori–Tanaka; Kerner's; H–T, Halpin–Tsai; S–L, Shen–Li.

Several models are available in the literature to account for the increase of elastic moduli with the presence of filler particles. Notable examples are the models by Kerner,[22] Hashin[23] and Christensen's three-phase model.[20] Models that are not limited to spherical particles but that take into account the aspect ratio of the filler particles, such as the Mori-Tanaka model, can also be found.[24] This model can be applied to this case considering the limit in which the aspect ratio equals the unity. Table 3 lists all the calculations and values of the properties for the pure materials that were used.

It was found that for the relatively low volume fractions of filler used, all of these methods yield predictions for the Young's modulus of the composite which are very close to each other, but that are consistently and significantly below

Table 3. Material properties of polymer matrix and filler

Sample	Young's modulus, E (GPa)	Poisson's ratio, ν	Thermal expansion
PA6	2.750	0.4	90 ($\times 10^{-6}\,K^{-1}$)
Silica	73.1	0.17	0.55 ($\times 10^{-6}$/°C) at 300 K

the values measured experimentally, as is shown in Figs. 11 and 12. There are many factors that are responsible for these limitations, some of which have been discussed previously by other authors. One of the possibilities is the formation of an interface between the filler particle and the matrix. However, in the present case, until firm evidence of such an interface is found, this modification may be regarded only as a means to compensate for the limitations of the models.

Very recently Shen and Li developed a model, which takes the the presence of an inhomogeneous interface into account.[25] In this theory, the mechanical properties of medium at the microscopic scale do not change abruptly at the interface between the spherical particle and the polymeric matrix, but a transition region (or interface) exists, in which the properties continuously relax until reaching the properties of the pure matrix at sufficiently long distances from the center of the filler particle. A particle together with its surrounding interface is called a composite sphere. If r_0 and r_1 denote the radii of the particle and the composite sphere, respectively, and $C_{eff}/(r)$ the effective properties of the composite sphere with radius $r \in [r_0, r_1]$, then the effective modulus of the particle-reinforced medium with an inhomogeneous interface can be evaluated as:

$$\frac{C}{C_m} = 1 + \frac{\phi}{C_m/[C_{eff}(r_1) - C_m] + (1-\phi)\alpha_m^C} \tag{5}$$

where $\phi = \phi_f(r_1/r_0)^3$ and α_m^C depends on the particular modulus to be evaluated and is given by:

$$\alpha_m^k = \frac{1+\nu^m}{3(1-\nu^m)} \tag{6}$$

in the case of the bulk modulus, and by:

$$\alpha_m^\mu = \frac{8-10\nu^m}{15(1-\nu^m)} \tag{7}$$

in the case of the shear modulus.

The function C_{eff} (r) satisfies the following differential equation:

$$\frac{dC_{eff}(r)}{dr} = -\frac{3}{r}\left[[C_{eff}(r) - C_i(r)] + \frac{\alpha_m^C}{C_i}[C_{eff}(r) - C_i(r)]^2\right], \tag{8}$$

subject to the initial condition C_{eff} $(r_0) = C_f$

Following the Shen–Li model the following formula was used for the radial dependence of the Young modulus at the interface:

$$\frac{E_i(r)}{E_m} = 1 - D\left(\frac{r}{r_0}\right)^{-\beta} \tag{9}$$

with the so-called 'damage parameter' $D = -0.5$, and the parameter β was chosen to best represent the experimental data. Equation (8) is integrated numerically from $r = r_0$ to $r = r_1$ sufficiently large to ensure convergence of $C_{eff}(r)$. This value was then substituted in eqn. (5).

At points sufficiently far away from the particle surface, the properties are equal to those of the matrix. The exponent β is a measure of the width of the region in which the properties are substantially different to that of the pure matrix. Reasonable agreement was found with experimental data obtained, $\beta = 2.9$ for the polymer composite. The values of the

β parameter correspond to a transition which ends approximately at $r_1/r_0 = 1.74$ for the polymer composites.

Another way to represent the data is through the use of a semi-empirical model. Halpin and Tsai[26] developed a widely used semi-empirical equation, which was later generalized by Nielsen.[19] For our purposes the following forms were used:

$$\frac{C}{C_m} = \frac{1 + \xi\phi_f}{1 - \eta\phi_f}$$

where

$$\eta = \frac{(E_f/E_m) - 1}{(E_f/E_m) + \xi}$$

and ξ is treated as a curve fitting parameter which is a measure for the degree of reinforcement of the matrix by the filler.[27] Best agreement with measured values of the Young's modulus and those calculated with the Shen–Li model was obtained with $\xi = 7.3$ for the polymer composites.

CONCLUSIONS

Nylon-6/silica nanocomposites were prepared by devolatilization technique for the first time. The filler used was added as sol in a twin-screw extruder apparatus instead of the *in situ* polymerization technique, providing bulk amounts of composite material at industrial scale. After the first heating rate the enthalphy of crystallization increased and the XRD spectra showed a constant degree of crystallinity for all the composites. The behavior illustrated with the DMA curves indicated that in general when a filled system is compared to an unfilled material, the values of the moduli (E' and E'') increased and damping decreased. Furthermore, the values measured experimentally are found to be above of the theoretical predictions.

Additionally, the production of (nano)-composites using this method brings new insights to the properies of PA-filled materials.

Acknowledgments

This work was financially supported by the Netherlands Organization for Scientific Research (NWO-PPM), and we thank Professor S. Picken for helpful discussion.

REFERENCES

1. Kojima Y, Usuki A, Kawasumi M, Okada A, Kurauchi T, Kamigaito O. Sintesis of nylon 6-clay hybrid by montmorillonite intercalated with ε-caprolactam. *J. Polym. Sci., Part A*. 1993; **31**: 983.
2. Merkel TC, Freemanzz BD, Spontak RJ, He Z, Pinnau I, Meakin P, Hill AJ. Ultrapermeable, reverse-selective nanocomposite membranes. *Science* 2002; **296**: 519.
3. Kohan MI. *Nylon, Plastics Handbook*. Hanser: New York, 1995.
4. Ou Y, Yang F, Yu Z-Z. A new conception on the toughness of nylon 6-silica nanocomposite prepared via *in situ* polymerization. *J. Polym. Sci*. 1998; **5**: 789.
5. Wypych G. *Handbook of Fillers* (2nd edn). Hanser: New York, 1985.
6. Brook MA. *Silicon in Organic, Organometallic, and Polymer Chemistry*. John Wiley & Sons: New York, 2000.
7. Rothon R. *Particulate-filled Polymer Composites*. Essex: Longman, 1995.
8. Li Y, Yu J, Guo Z. The influence of silane treatment on nylon-6/nano-SiO_2 by *in situ* polymerization. *J. Appl. Polym. Sci*. 2002; **84**: 827.
9. Reynaud E, Jouen T, Gauthier C, Vigier G, Varlet J. Nanofillers in polymeric matrix: a study on silica reinforced PA-6. *Polymer* 2001; **42**: 8759.
10. Petrović ZS, Javni I, Waddon A, Bánhegyi G. Structure and properties of polyurethane-silica nanocomposites. *J. Appl. Sci*. 2000; **76**: 133.
11. Nielsen LE. Dynamic mechanical properties of polymer filled with agglomerated particles. *J. Polym. Sci.: Polym Phys*. 1979; **17**: 1897.
12. Sumita M, Shizuma T, Miyasaka K. Effect of reducible properties of temperature, rate of strain, and filler content on the tensile yield stress of nylon-6 composites filled with ultrafine particles. *J. Macromol. Sci. Phys*. 1983; **B22**(4): 601.
13. Bussi P, Thierry-Mieg J. *Polymer filled with Solid Particles*. US Patent 6,239,196 B1, 2001.
14. Li W, Yan D. Synthesis and characterization of nylons based on hexadecane diacid. *J. Appl. Polym. Sci*. 2003; **88**: 2462.
15. Yang F, Ou Y, Yu Z. Polyamide 6/silica nanocomposites prepared by *in situ* polymerization. *J. Appl. Polym. Sci*. 1998; **69**: 355.
16. Gagliardi S, Arrighi V, Ferguson R, Telling MTF. Restricted dynamics in polymer-filler systems. *Physica B* 2001; **301**: 110.
17. Lewis TB, Nielsen LE. Dynamic mechanical properties of particulate-filled composites. *J. Appl. Polym. Sci*. 1970; **14**: 1449.
18. Nielsen LE. Dynamic mechanical properties of polymer filled with agglomerated particles. *J. Polym. Sci*. 1979; **17**: 1897.
19. Nielsen LE, Lewis TB. Temperature dependence of relative modulus in filled polymer systems. *J. Appl. Polym. Sci*. 1969; **7**: 1705.
20. Christensen RM. *Mechanics of Composite Materials*. John Wiley & Sons: Chichester, 1979.
21. Nielsen LE, Landel RF. *Mechanical Properties of Polymers and Composites* (12th edn). Marcel Dekker: New York, 1994.
22. Kerner EH. The elastic and thermo-elastic properties of composite media. *Proc. Phys. Soc*. 1956; **B69**: 808.
23. Hashin Z. Thermoelastic properties of particulate composites with imperfect interfaces. *J. Mech. Phys. Sol*. 1991; **39**: 745.
24. Mori T, Tanaka K. Average stress in matrix and average elastic energy of materials with misfitting inclusions. *Acta Metal*. 1973; **21**: 571.
25. Shen L, Li J. Effective elastic moduli of composites reinforced by particle or fiber with an inhomogeneous interphase. *Int. J. Solids Struct*. 2003; **40**: 1393.
26. Halpin JC, Tsai SW. *Effects of environmental factors on composite materials*. AFML-TR-67-423 June 1969.
27. Gibson RF. *Principles of Composite Material Mechanics*. McGraw Hill: London, 1994.